ACS APPLIED MATERIALS & INTERFACES

Letter

www.acsami.org

Solution-Processed CdS/Cu_2S Superlattice Nanowire with Enhanced Thermoelectric Property

Ze Xiong,[†,§] Yu Cai,[†,§] Xiaodong Ren,[‡] Bei Cao,[†,∥] Jianjun Liu,[#] Ziyang Huo,[*,⊥] and Jinyao Tang[*,†]

[†]Department of Chemistry, The University of Hong Kong, Hong Kong 999077, China

[‡]State Key Laboratory of Functional Materials for Informatics, Shanghai Institute of Microsystem and Information Technology, Chinese Academy of Sciences, Shanghai 200050, China

[∥]State Key Laboratory of Synthetic Chemistry, The University of Hong Kong, Hong Kong 999077, China

[#]State Key Laboratory of High-Performance Ceramics and Super Fine Microstructures, Shanghai Institute of Ceramics, Chinese Academy of Sciences, Shanghai 200050, China

[⊥]Queensland Micro- and Nanotechnology Center, Nathan Campus, Griffith University, Brisbane 4111, Australia

Supporting Information

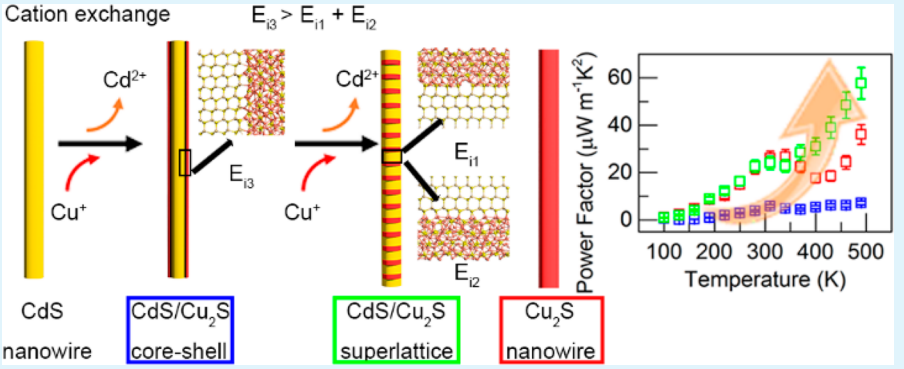

ABSTRACT: Previously, the solution-based cation exchange reaction has been extensively studied for the synthesis of the complex heteroepitaxial nanocolloidals. Here, we demonstrated that the strain induced selective phase segregation technique can also be applied to large size nanowires in a well-studied CdS/Cu_2S system, leading to the formation of superlattice nanowire structure with a simple solution-based cation exchange reaction. This structural evolution is driven by the distinct interface formation energy at different CdS facets as indicated by ab initio calculation. Because of the energy filtering effect, the superlattice nanowire shows an enhanced thermopower without significant decrease of the electrical conductivity. This study provides a promising low-cost solution process to produce superlattice nanostructures for practical thermoelectric applications.

KEYWORDS: *cation exchange reaction, nanowire, self-assembly, superlattice, thermoelectric applications*

It is well-known that the strain originated from the large lattice mismatch at the heteroepitaxial interface often leads to uncontrollable interface defects formation in two-dimensional thin films. In contrast, the lattice mismatch strain in nanocolloidals with the size of a few nanometers may result in controllable phase segregation that facilitated the synthesis of many complex nanostructures such as CdS/Ag_2S superlattice[1] and CdS/Cu_2S asymmetric binary nanocolloidals[2] via simple cation exchange reactions.[3] Similarly, the cation exchange chemistry on nanowires with diameter around 100 nm has also been extensively explored.[4,5] However, because of the large crystal size and slow ion diffusion, the cation exchange reaction does not seem to be a viable method for complex heterojunction nanowires synthesis besides coaxial nanowires.[6] On the other hand, inspired by pioneering theoretical[7−11] and experimental studies,[12−15] the heterojunction superlattice nanowire was suggested to be a promising thermoelectric material due to the quantum confinement, the energy filtering effect, and the interface phonon scattering, which simultaneously offers the thermopower enhancement and the thermal conductivity reduction without significant deteriorate the electrical conductivity. In order to achieve the composition alternation for heterosuperlattice nanowires, a sequential deposition growth is usually applied.[16−18] However, in this process, because each inclusion layer inside the nanowire requires a switching of the composition of the precursors, this technique is not desired for large scale synthesis and thermoelectric application where superlattices with many inclusion layers are desired. Recently, the high temperatures controllable phase segregation technique was developed in the

Received: June 28, 2017
Accepted: September 13, 2017
Published: September 13, 2017

DOI: 10.1021/acsami.7b09346
ACS Appl. Mater. Interfaces XXXX, XXX, XXX−XXX

gold−germanium nanowire,[19] whereas other self-assembly-based techniques for thermoelectric related superlattice nanowire still need to be developed in other material systems. Furthermore, compared to the well-observed thermal conductivity suppression in superlattice nanostructures,[17,20] the experimental demonstration of the proposed thermopower enhancement is rarely reported.

Herein, we report a simple solution-based process to synthesize CdS/Cu_2S superlattice nanowires by Cu^+ cation exchange with physical vapor deposition (PVD) grown CdS nanowire and the enhanced thermoelectric performance of the resulting superlattice nanowires. Upon Cd^{2+} replaced by Cu^+ in CdS nanowires, the core−shell CdS/Cu_2S nanowire with low surface defect density was first produced.[6] With further Cu^+ diffusion into the CdS nanowire core, the lattice mismatch induced strain is built up and prevents the further growth of the conformal Cu_2S shell. Instead, the CdS/Cu_2S nanowire is converted into a superlattice structure, similar to the CdS/Ag_2S superlattice discovered in the much smaller nanocolloidal system.[1] Such phase evolution of Cu_2S/CdS can be explained by the distinct interface formation energies of CdS/Cu_2S attachments at different CdS facets as indicated in ab initio calculation. Moreover, this solution-processed CdS/Cu_2S superlattice nanowire exhibits an enhanced thermopower over pure Cu_2S nanowire and CdS/Cu_2S core−shell nanowire due to energy filtering effect, which provides a potential route to designing high-performance thermoelectric superlattice nanowire materials.

In our experiment, the CdS nanowires were first synthesized by PVD method described previously,[21] where a 20 nm gold thin film was utilized as catalyst (Supporting Information). The as-synthesized CdS nanowires with diameters ranging from 80 to 200 nm and lengths up to 100 μm are used for further cation exchange reaction. The X-ray diffraction (XRD) pattern matches very well with wurtzite phase CdS with a strong (0002) peak, indicating a preferential nanowire growth along the ⟨0002⟩ direction (Figures S1 and S2). Then, the CdS nanowires were dipped into 0.5 M CuCl solution at 80 °C for the different durations for cation exchange reaction (0−30 min) and examined with high-resolution transmission electron microscopy (HRTEM). As shown in Figure 1a, the phase evolution proceeds from pristine CdS nanowire to CdS/Cu_2S core−shell nanowire, and eventually to CdS/Cu_2S superlattice nanowire. Correspondingly, the X-ray diffraction results show that the CdS (0002) peak gradually diminishes with increasing reaction time, whereas the low-temperature phase of chalcocite Cu_2S (L-Cu_2S) peaks noticeably emerge after 3 min of reaction (Figure S1). Nevertheless, the CdS (1000) and (10$\bar{1}$1) peaks do not completely disappear even after 30 min reaction. Compared to the complete cation exchange conversion into Cu_2S nanowire in thin CdS nanowire,[4] the incomplete convertion in our large diameter nanowires implies that the slow diffusion kinetics of Cd^{2+} ions could be the rate limiting step in the cation exchange reaction.

The more detailed inspection of the TEM image shows the progression of the cation exchange reaction. After 0.5 min of reaction, a CdS/Cu_2S core−shell structure can be observed with a Cu_2S shell thickness of ∼5 nm (Figure 1c). At this stage, the Cu_2S layer is below the critical thickness, and the strain induced by lattice mismatch can be relaxed without creating interface defects. With reaction time over 3 min, the Cu_2S inclusion layers were observed in the nanowire, and the CdS/Cu_2S superlattice structure is formed (Figures 1d, 2a and Figure S3). The Cu element electron energy loss spectrum (EELS) mapping image confirmed this superlattice structure (Figure 2b), which shows the copper-rich inclusion layers in CdS matrix. In order to get more in-depth information and atomic resolution image of the inclusion Cu_2S layers, the superlattice nanowires were dipped into 0.1 M HCl for 15 min to etch away the CdS segments selectively. Because the Cu_2S is insoluble in dilute HCl, the Cu_2S sections were left intact (Figure 2c), whereas most of the CdS sections are removed selectively. Figure 2d gives the corresponding EELS elemental mapping image for Cu element, indicating the long-range ordering of the superlattice structure. The high-resolution TEM image of the Cu_2S inclusion layers shows good single crystallinity (Figure 2e), which agrees well with the XRD results of crystalline L-Cu_2S phase. It is well-known that Cu_2S and CdS form type II heterojunction that is excellent for photoexcited charge separation.[6] As shown in Figure 2f, the photoluminescence (PL) measurements of the pristine CdS nanowire shows strong typical band edge emission with the peak wavelength at 500 nm. Upon cation exchange reaction for a short time (0.5 min), the core−shell CdS/Cu_2S shows a much-suppressed band edge emission of CdS, which indicates the incomplete exciton extraction at the CdS/Cu_2S interface. With the formation of superlattice CdS/Cu_2S nanowires (3 min reaction time), the PL is dramatically quenched because of the enhanced exciton separation at the interface,[1] leaving a broad broadband emission with the peak wavelength around 570 nm.

To rationalize the conversion from core−shell nanowire to superlattice in CdS/Cu_2S cation exchange reaction, the

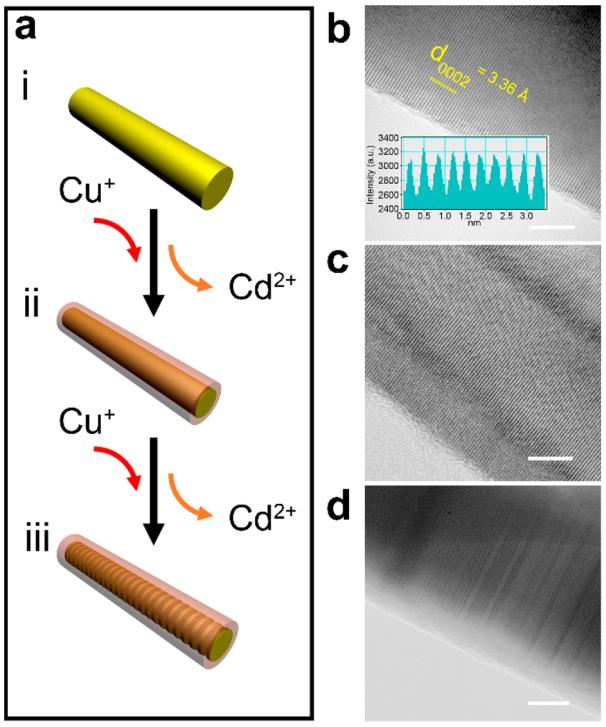

Figure 1. (a) Schematic diagram of phase evolution from pristine CdS nanowire to CdS/Cu_2S core−shell nanowire, and eventually to CdS/Cu_2S superlattice nanowire. TEM images of (b) pristine CdS nanowire, (c) CdS/Cu_2S core−shell nanowire and (d) CdS/Cu_2S superlattice nanowire. Inset: transmitted electron intensity profile along the periodic spacing denoted by yellow line, which is consistent with the lattice distance (∼3.36 Å) of wurtzite phase CdS (0002) plane. Scale bars: (b, c) 5 nm; (d) 30 nm.

DOI: 10.1021/acsami.7b09346
ACS Appl. Mater. Interfaces XXXX, XXX, XXX−XXX

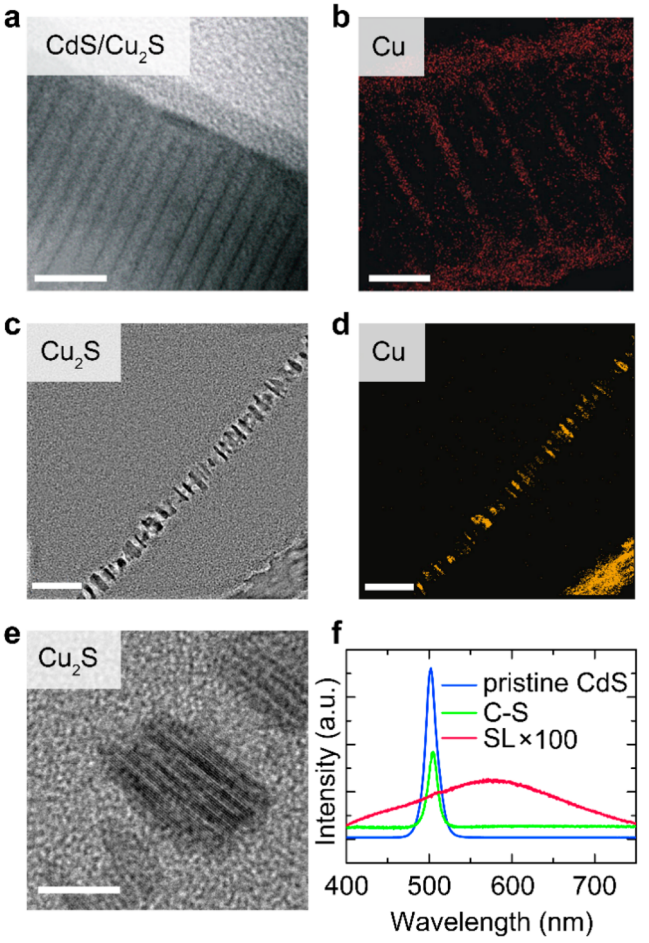

Figure 2. CdS/Cu_2S superlattice nanowire characterizations. (a) TEM and corresponding (b) Cu EELS elemental mapping images of CdS/Cu_2S superlattice nanowire. Scale bar: 20 nm. (c) TEM and (d) Cu EELS mapping images of CdS/Cu_2S superlattice nanowire after removal of CdS by 0.1 M HCl. Scale bar: 50 nm. (e) High-resolution TEM image of Cu_2S region after removal of CdS by 0.1 M HCl. Scale bar: 10 nm. (f) PL spectra of single pristine CdS nanowire, as-prepared CdS/Cu_2S core–shell nanowires (C–S) and CdS/Cu_2S superlattice nanowires (SL). For clarity, the intensity of CdS/Cu_2S superlattice nanowires is multiplied by 100.

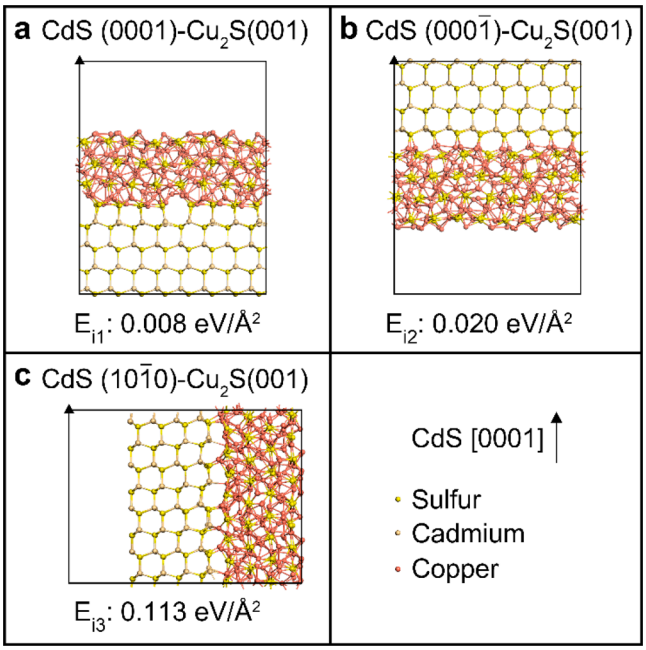

Figure 3. Models and interface formation energies (E_i) for the CdS–Cu_2S interfaces in the superlattice nanowire. (a) CdS (0001)–Cu_2S (001) and (b) CdS (000$\bar{1}$)–Cu_2S (001) interfaces, parallel to the nanowire cross section. (c) CdS (10$\bar{1}$0)–Cu_2S (001) interface, parallel to the length of the nanowire. The E_i is depicted as eV per unit interfacial area.

formation energies of CdS–Cu_2S interfaces at different facets of CdS nanowire are calculated to evaluate their relative stability. Because the sulfur sublattice in Cu_2S has a small mismatch with the hexagonal close-packed sulfur sublattice in CdS,[22] the interfaces can be made by treating the Cu_2S as pseudo-orthorhombic for easier modeling (Table S1, Figure S4), albeit the unit cell of L-Cu_2S is monoclinic.[23] The models of epitaxial attachments between wurtzite CdS and L-Cu_2S are shown in Figure 3. The formation energies at CdS (0001) (E_{i1} = 0.008 eV/Å^2) and (000$\bar{1}$) (E_{i2} = 0.020 eV/Å^2) facets, which are the normal surface to the nanowire growth direction, are much less than that at the CdS (10$\bar{1}$0) (E_{i3} = 0.113 eV/Å^2) facet that is along the nanowire growth direction (Figure 3). As a result, it is thermodynamically favorable to form the Cu_2S/CdS interface perpendicular to the nanowire growth direction[4] rather than Cu_2S shells.

We propose that the lattice mismatch strain at CdS/Cu_2S interface drives the conversion of the core–shell nanowire into a superlattice structure during the cation exchange reaction. A critical thickness ~23.9 nm corresponding to the formation of the line dislocation in the core–shell structure can be estimated based on the theoretical analysis of strained heterojunctions,[24,25] which align with the observed Cu_2S shell thickness (<20 nm) in our samples. After the initial formation of CdS/Cu_2S core–shell structure, the strain near the CdS–Cu_2S interface increases with growing Cu_2S shell thickness, which leads to the instability of the epitaxial interface and forms dislocation defects when approaching the critical thickness. Similar to the Stranski–Krastanov growth on the two-dimensional surface,[26] where the semiperiodic nanoparticle islands are formed on heteroepitaxial thin film for excess stress relaxation, the semiperiodic dislocation defects can be generated by cation exchange reaction on the CdS/Cu_2S core–shell nanowire. Because of the lower formation energies at CdS (0001)–Cu_2S (001) and CdS (000$\bar{1}$)–Cu_2S (001) interfaces, the dislocation defects serve as the initiating sites where the Cu_2S crystals grow into the CdS core at the expense of the outer Cu_2S shell until the Cu_2S span the entire diameter of CdS nanowire and form the semiperiodic inclusion layers in the nanowire. After formation of the superlattice nanowire, the further cation exchange is slowed down due to the slow diffusion of Cd^{2+} inside the nanowire, which prevents the complete conversion to pure Cu_2S nanowire as observed in nanowires with a smaller diameter.[4] Similarly, the lattice mismatch strain also facilitates the Cu_2S formation at the ends of CdS nanowires with a smaller diameter, as have been reported in previous studies.[2,4] The core–shell nanowire to superlattices conversion could cease when the Cu_2S shell thickness decrease below the critical thickness, and the strain is greatly relaxed. This metastable superlattice nanowire with remained Cu_2S shell can occasionally be observed in TEM (Figure S5).

With this solution-processed superlattice nanowire, we investigated the thermopower enhancement as predicted by

DOI: 10.1021/acsami.7b09346
ACS Appl. Mater. Interfaces XXXX, XXX, XXX–XXX

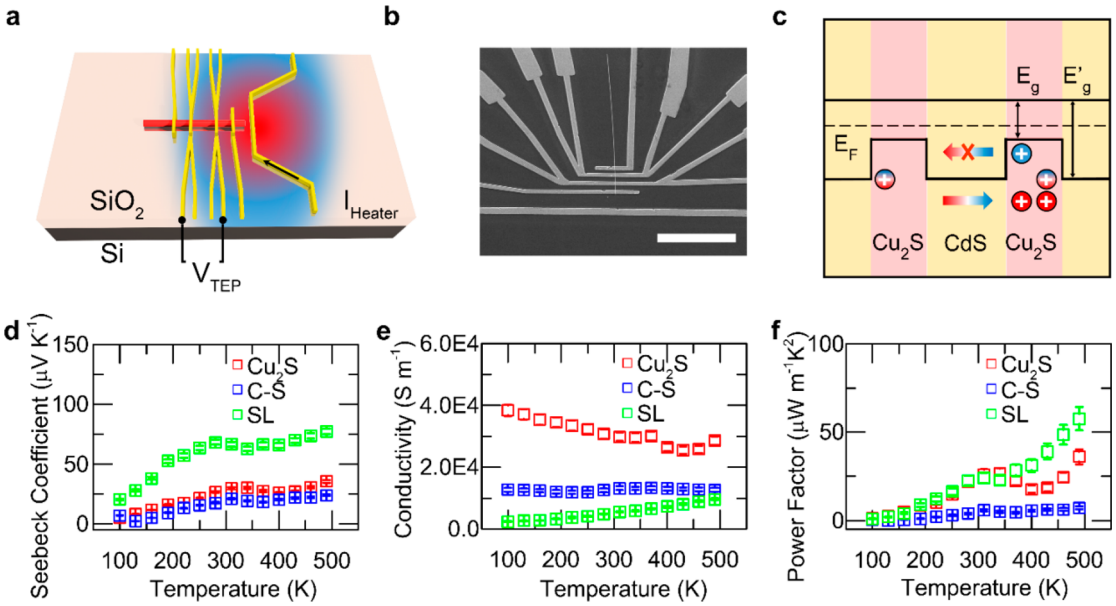

Figure 4. Temperature dependence of thermoelectric properties of Cu_2S nanowire, CdS/Cu_2S core−shell nanowires (C−S) and CdS/Cu_2S superlattice nanowires (SL). (a) The illustration for the thermoelectric properties measurement. (b) SEM image of the fabricated device for thermopower measurement. Scale bar: 30 μm. (c) Schematic diagram of carrier energy filtering for power factor enhancement. (d) Thermopower. (e) Electrical conductivity. (f) Power factor of nanowires. With consideration of the measurement error from both σ (3.5%) and S (4%), the power factor shows 11.5% uncertainty at 95% confidence.

energy filtering effect.[7,9,10] The enhanced thermopower roots in the energy filtering affect which preferentially traps the low energy carriers.[12] To measure the thermoelectric properties of our CdS/Cu_2S superlattice nanowire, the nanowire is electrically connected to two electrodes that also serve as the temperature sensors. With a temperature gradient (ΔT) created by a DC current over a nearby heating electrode, a thermovoltage (V_{TEP}) can be generated along the nanowire and the thermopower S can be calculated as $S = -V_{TEP}/\Delta T$ (Figure 4a,b). Here, we focused on the electrical part of the thermoelectric properties of superlattice nanowire and compared it to the core−shell CdS/Cu_2S nanowire and pure Cu_2S nanowire. Because of the complete conversion from CdS to Cu_2S nanowire cannot be achieved in our large diameter nanowires even with prolonged reaction time, high quality single crystalline Cu_2S nanowires were synthesized by single precursor solution−liquid−solid (SLS) method for the comparison of the thermoelectric properties (Figure S6).

In CdS/Cu_2S superlattice nanowire, the alternating CdS and Cu_2S layers form a typical type II semiconductor junction as shown in Figure 4c.[27] It is known that the cation exchange reaction produces near-degenerately doped p^+-Cu_2S with carrier concentration around 10^{20} cm^{-3}.[28] When contact with near intrinsic CdS produced by PVD method, the band bending almost entirely reside in CdS layer. Because the CdS layer is only a few nanometers thick, the high concentration holes in Cu_2S diffuse through the CdS layer and result in a high hole conductivity in CdS layers. As a result, the superlattice nanowire appears as a p-type semiconductor with periodic energy barrier primarily contributed from the valence band offset between two materials, which causes the energy filtering effect. Upon experiencing temperature gradient along the superlattice nanowire, the "hot carriers" with higher thermal energy can diffuse over the energy barrier to the lower temperature region while the "cold carriers" are preferentially trapped, which will effectively inhibit the back diffusion of carriers and enhance the thermopower of the superlattice nanowire.[12]

As shown in Figure 4d, the positive thermopower S confirms that the holes indeed serve as the majority carriers in all the samples. In the core−shell nanowire produced by short time cation exchange reaction, the transport behavior is dominated by the highly conductive Cu_2S shell. Therefore, the CdS/Cu_2S core−shell nanowire and pure Cu_2S nanowire display very similar thermopower across the entire temperature region. With the Cu_2S inclusion layers inside the superlattice nanowire, the thermopower will be improved due to the transport of carriers through the CdS and Cu_2S layers. It is noteworthy that the dampened S around 400 K in Cu_2S and CdS/Cu_2S core−shell nanowires is caused by the transition of Cu_2S from monoclinic low-chalcocite (LC) to hexagonal high-chalcocite (HC) phase.[29] In contrast, the transition of S in CdS/Cu_2S superlattice nanowire is more pronounced and significantly shifted to lower temperature (~330 K). This observation can be well explained by the size dependence of the temperature-induced solid−solid phase transition as reported in Cu_2S nanorod.[30] As the critical length of the Cu_2S nanorod decreased to ~5 nm, the LC-HC transition temperature is reduced to ~330 K, which aligns with the TEM result of our superlattice nanowire where the Cu_2S inclusion thickness is also around 5 nm. Because the barrier height in our superlattices is about 1.2 eV,[27] which is too large to keep the majority carrier mobility without degradation, the electrical conductivity σ of superlattice nanowire was suppressed compared to the CdS/Cu_2S core−shell and pure Cu_2S nanowire (Figure 4e). Furthermore, we noticed that some defects formed in the CdS/Cu_2S superlattice nanowire after cation exchange reaction that induce many structural failures in our nanowires and could also deteriorate σ of the measured nanowires. Nevertheless, the superlattice nanowire still shows an enhanced power factor σS^2 beyond 400 K (Figure 4f), which can be further improved by lowering the energy barrier height via different materials combination such

DOI: 10.1021/acsami.7b09346
ACS Appl. Mater. Interfaces XXXX, XXX, XXX−XXX

as CdSe/Cu_2Se and finely controlling the reaction condition for higher material integrity.

In conclusion, a simple aqueous solution-processed cation exchange approach has been demonstrated to convert the PVD-grown CdS nanowires into CdS/Cu_2S superlattice structure. The evolution of CdS from nanowire to core−shell CdS/Cu_2S structure and to CdS/Cu_2S superlattice nanowire can be explained by the distinct interface formation energy at different CdS facets and the self-regulated strain energy relaxation at the CdS−Cu_2S interface. The energy filtering effect favored by the junction formed at the CdS−Cu_2S interface can significantly enhance the thermopower without greatly undermining the electrical conductivity of the superlattice nanowires, which provides an enhanced power factor compared to pure Cu_2S nanowires. Considering the well demonstrated thermal conductivity suppression due to the phonons boundary scattering in superlattice nanowires,[17] an improvement of the *ZT* value of the CdS/Cu_2S superlattice nanowires is expected, which could serve as promising materials for refrigeration application under room temperature or for the power generation to harvest the waste heat from automobile and industrial combustion processes under higher temperature (>400 K).

■ ASSOCIATED CONTENT

Supporting Information

The Supporting Information is available free of charge on the ACS Publications website at DOI: 10.1021/acsami.7b09346.

Experimental and VASP modeling details, XRD of CdS and CdS/Cu_2S nanowires, low-temperature chalcocite Cu_2S structure information, TEM of HCl etched CdS/Cu_2S superlattice nanowires, SEM and XRD of pure Cu_2S nanowires (PDF)

■ AUTHOR INFORMATION

Corresponding Authors

*Z.H. E-mail: ziyanghuo@gmail.com.
*J.T. E-mail: jinyao@hku.hk.

ORCID

Jinyao Tang: 0000-0002-0051-148X

Author Contributions

§These authors contributed equally to this work.

Notes

The authors declare no competing financial interest.

■ ACKNOWLEDGMENTS

This work was supported in part by the Hong Kong Research Grants Council (RGC) General Research Fund (GRF17303015, GRF17305917, ECS27300814), the University Grant Council (Contract No. AoE/P-04/08), the URC Strategic Research Theme on Clean Energy (University of Hong Kong), and the URC Strategic Research Theme on New Materials (University of Hong Kong).

■ REFERENCES

(1) Robinson, R. D.; Sadtler, B.; Demchenko, D. O.; Erdonmez, C. K.; Wang, L.-W.; Alivisatos, A. P. Spontaneous Superlattice Formation in Nanorods through Partial Cation Exchange. *Science* **2007**, *317* (5836), 355−358.

(2) Sadtler, B.; Demchenko, D. O.; Zheng, H.; Hughes, S. M.; Merkle, M. G.; Dahmen, U.; Wang, L. W.; Alivisatos, A. P. Selective Facet Reactivity During Cation Exchange in Cadmium Sulfide Nanorods. *J. Am. Chem. Soc.* **2009**, *131* (14), 5285−5293.

(3) Beberwyck, B. J.; Surendranath, Y.; Alivisatos, A. P. Cation Exchange: A Versatile Tool for Nanomaterials Synthesis. *J. Phys. Chem. C* **2013**, *117* (39), 19759−19770.

(4) Zhang, D.; Wong, A. B.; Yu, Y.; Brittman, S.; Sun, J.; Fu, A.; Beberwyck, B.; Alivisatos, A. P.; Yang, P. Phase-Selective Cation-Exchange Chemistry in Sulfide Nanowire Systems. *J. Am. Chem. Soc.* **2014**, *136* (50), 17430−17433.

(5) Zhang, B.; Jung, Y.; Chung, H.-S.; Vugt, L. V.; Agarwal, R. Nanowire Transformation by Size-Dependent Cation Exchange Reactions. *Nano Lett.* **2010**, *10* (1), 149−155.

(6) Tang, J.; Huo, Z.; Brittman, S.; Gao, H.; Yang, P. Solution-Processed Core-Shell Nanowires for Efficient Photovoltaic Cells. *Nat. Nanotechnol.* **2011**, *6* (9), 568−572.

(7) Hicks, L. D.; Dresselhaus, M. S. Effect of Quantum-Well Structures on the Thermoelectric Figure of Merit. *Phys. Rev. B: Condens. Matter Mater. Phys.* **1993**, *47* (19), 12727−12731.

(8) Hicks, L. D.; Dresselhaus, M. S. Thermoelectric Figure of Merit of a One-Dimensional Conductor. *Phys. Rev. B: Condens. Matter Mater. Phys.* **1993**, *47* (24), 16631−16634.

(9) Whitlow, L. W.; Hirano, T. Superlattice Applications to Thermoelectricity. *J. Appl. Phys.* **1995**, *78* (9), 5460−5466.

(10) Vashaee, D.; Shakouri, A. Improved Thermoelectric Power Factor in Metal-Based Superlattices. *Phys. Rev. Lett.* **2004**, *92* (10), 106103.

(11) Neophytou, N.; Kosina, H. Optimizing Thermoelectric Power Factor by Means of a Potential Barrier. *J. Appl. Phys.* **2013**, *114* (4), 044315.

(12) Andrews, S. C.; Fardy, M. A.; Moore, M. C.; Aloni, S.; Zhang, M. J.; Radmilovic, V.; Yang, P. D. Atomic-Level Control of the Thermoelectric Properties in Polytypoid Nanowires. *Chem. Sci.* **2011**, *2* (4), 706−714.

(13) Snyder, G. J.; Toberer, E. S. Complex Thermoelectric Materials. *Nat. Mater.* **2008**, *7* (2), 105−114.

(14) Bulman, G.; Barletta, P.; Lewis, J.; Baldasaro, N.; Manno, M.; Bar-Cohen, A.; Yang, B. Superlattice-Based Thin-Film Thermoelectric Modules with High Cooling Fluxes. *Nat. Commun.* **2016**, *7*, 10302.

(15) Tian, R.; Wan, C.; Wang, Y.; Wei, Q.; Ishida, T.; Yamamoto, A.; Tsuruta, A.; Shin, W.; Li, S.; Koumoto, K. A Solution-Processed TiS_2/Organic Hybrid Superlattice Film Towards Flexible Thermoelectric Devices. *J. Mater. Chem. A* **2017**, *5* (2), 564−570.

(16) Gudiksen, M. S.; Lauhon, L. J.; Wang, J.; Smith, D. C.; Lieber, C. M. Growth of Nanowire Superlattice Structures for Nanoscale Photonics and Electronics. *Nature* **2002**, *415* (6872), 617−620.

(17) Li, D. Y.; Wu, Y.; Fan, R.; Yang, P. D.; Majumdar, A. Thermal Conductivity of Si/SiGe Superlattice Nanowires. *Appl. Phys. Lett.* **2003**, *83* (15), 3186−3188.

(18) Yoo, B.; Xiao, F.; Bozhilov, K. N.; Herman, J.; Ryan, M. A.; Myung, N. V. Electrodeposition of Thermoelectric Superlattice Nanowires. *Adv. Mater.* **2007**, *19* (2), 296−299.

(19) Chueh, Y. L.; Boswell, C. N.; Yuan, C. W.; Shin, S. J.; Takei, K.; Ho, J. C.; Ko, H.; Fan, Z. Y.; Haller, E. E.; Chrzan, D. C.; Javey, A. Nanoscale Structural Engineering Via Phase Segregation: Au-Ge System. *Nano Lett.* **2010**, *10* (2), 393−397.

(20) Chowdhury, I.; Prasher, R.; Lofgreen, K.; Chrysler, G.; Narasimhan, S.; Mahajan, R.; Koester, D.; Alley, R.; Venkatasubramanian, R. On-Chip Cooling by Superlattice-Based Thin-Film Thermoelectrics. *Nat. Nanotechnol.* **2009**, *4* (4), 235−238.

(21) Duan, X.; Lieber, C. M. General Synthesis of Compound Semiconductor Nanowires. *Adv. Mater.* **2000**, *12* (4), 298−302.

(22) Cook, W. R.; Shiozawa, L.; Augustine, F. Relationship of Copper Sulfide and Cadmium Sulfide Phases. *J. Appl. Phys.* **1970**, *41* (7), 3058−3063.

(23) Evans, H. T. Crystal Structure of Low Chalcocite. *Nature, Phys. Sci.* **1971**, *232*, 69−70.

(24) People, R.; Bean, J. C. Calculation of Critical Layer Thickness Versus Lattice Mismatch for Ge_xSi_{1-x}/Si Strained-Layer Heterostructures. *Appl. Phys. Lett.* **1985**, *47* (3), 322−324.

DOI: 10.1021/acsami.7b09346
ACS Appl. Mater. Interfaces XXXX, XXX, XXX−XXX

(25) Raychaudhuri, S.; Yu, E. T. Critical Dimensions in Coherently Strained Coaxial Nanowire Heterostructures. *J. Appl. Phys.* **2006**, *99* (11), 114308.
(26) Stangl, J.; Holý, V.; Bauer, G. Structural Properties of Self-Organized Semiconductor Nanostructures. *Rev. Mod. Phys.* **2004**, *76* (3), 725−783.
(27) Liu, G.; Schulmeyer, T.; Brötz, J.; Klein, A.; Jaegermann, W. Interface Properties and Band Alignment of Cu_2S/CdS Thin Film Solar Cells. *Thin Solid Films* **2003**, *431*−*432*, 477−482.
(28) Hmurcik, L.; Allen, L.; Serway, R. A. The Effects of Heat Treatments on the Transport Properties of Cuxs Thin Films. *J. Appl. Phys.* **1982**, *53* (12), 9063−9072.
(29) Chakrabarti, D. J.; Laughlin, D. E. The Cu-S (Copper-Sulfur) System. *Bull. Alloy Phase Diagrams* **1983**, *4* (3), 254−271.
(30) Rivest, J. B.; Fong, L.-K.; Jain, P. K.; Toney, M. F.; Alivisatos, A. P. Size Dependence of a Temperature-Induced Solid−Solid Phase Transition in Copper(I) Sulfide. *J. Phys. Chem. Lett.* **2011**, *2* (19), 2402−2406.

DOI: 10.1021/acsami.7b09346
ACS Appl. Mater. Interfaces XXXX, XXX, XXX−XXX